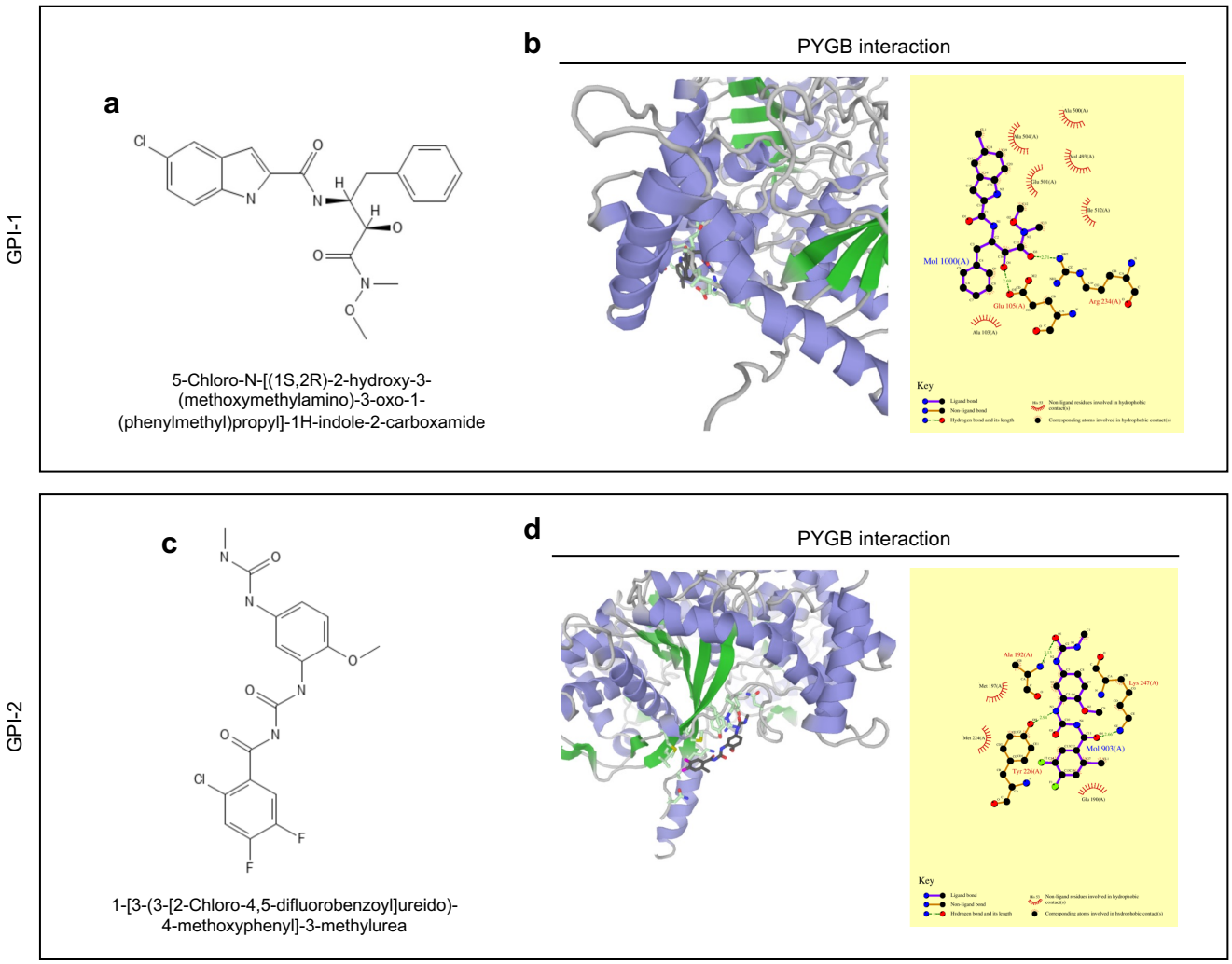


**Supplementary Figure 1. In-silico analysis of GPI - PYGB interaction.**

**a** Chemical structure of GPI-1 (Glycogen Phosphorylase Inhibitor - 1).

**b** 3D-structure of PYGB and GPI-1 binding (left). Binding pocket structure of PYGB and GPI-1 binding (right).

**c** Chemical structure of GPI-2 (Glycogen Phosphorylase Inhibitor - 2).

**d** 3D-structure of PYGB and GPI-2 binding (left). Binding pocket structure of PYGB and GPI-2 binding (right).

Protein-ligand docking interaction is analyzed by GalaxyDockWEB.

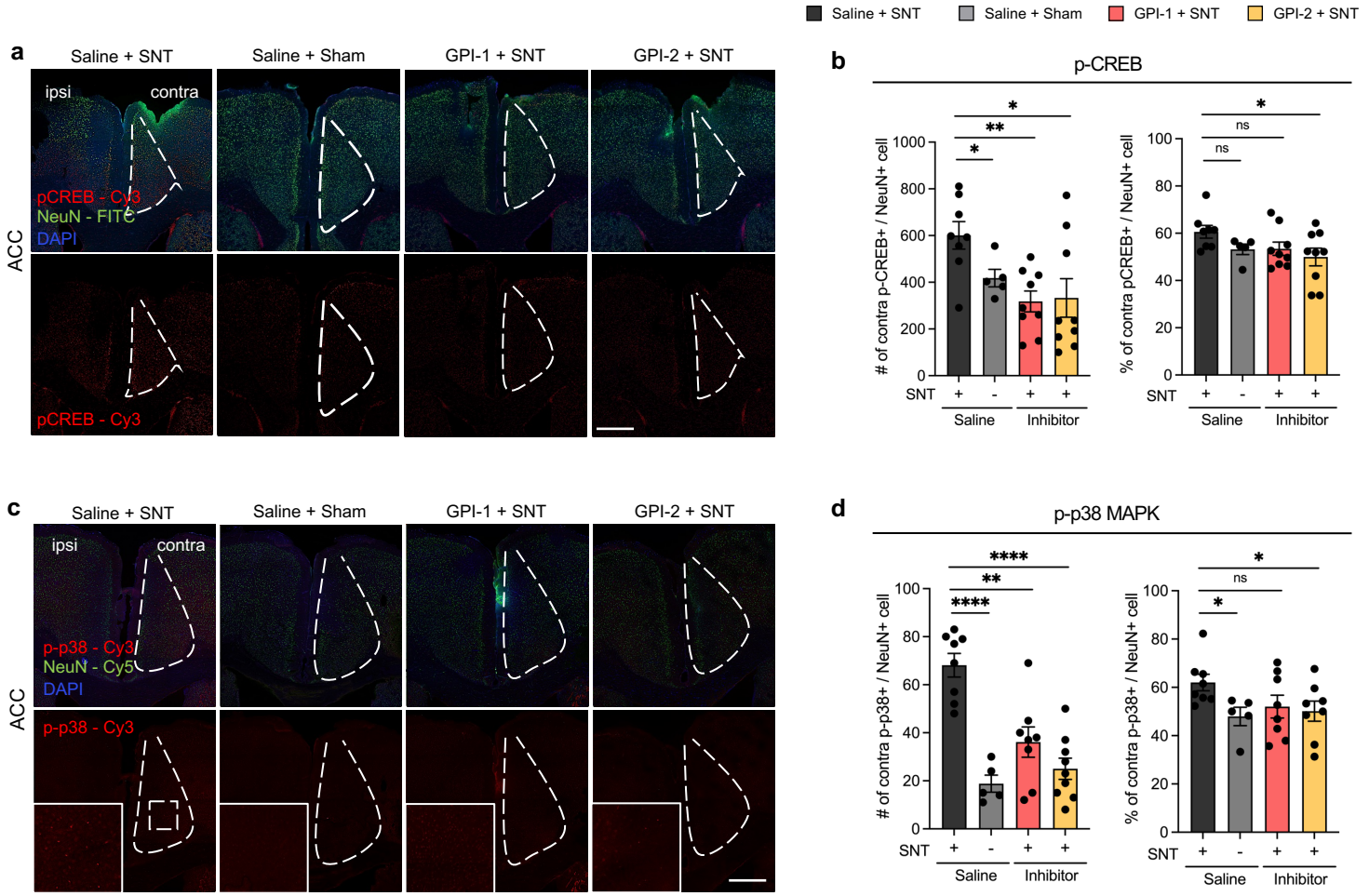


**Supplementary Figure 2. Inhibition of ACC glycogenolysis decreases neuronal activation in neuropathic pain chronification.**

**a-b** IHC data of p-CERB+/NeuN+ cell in ACC.

**a** Representative confocal images of ACC. (Scale bar, 200 μm)

**b** p-CERB+/NeuN+ cell counting analysis data. (Left): Number of p-CREB+/NeuN+ cell in ACC contra area. *P = 0.0451 (Saline + Sham verses Saline + SNT), **P = 0.0015 (GPI-1 + SNT verse Saline + SNT), *P = 0.0015 (GPI-2 + SNT verse Saline + SNT), (Right): Ratio of p-CREB+/NeuN+ cell in ACC contra area, compare with ipsi area. *P = 0.0390 (GPI-2 + SNT verse Saline + SNT)

**c-d** IHC data of p-p38+/NeuN+ cell in ACC.

**c** Representative confocal images of ACC. (Scale bar, 200 μm)

**d** p-p38+/NeuN+ cell counting analysis data. (Left): Number of p-p38+/NeuN+ cell in ACC contra area. ****P < 0.0001 (Saline + Sham verses Saline + SNT), **P = 0.0013 (GPI-1 + SNT verse Saline + SNT), ****P < 0.0001 (GPI-2 + SNT verse Saline + SNT), (Right): Ratio of p-p38+/NeuN+ cell in ACC contra area, compare with ipsi area. *P = 0.0218 (Saline + Sham verses Saline + SNT), *P = 0.0422 (GPI-2 + SNT verse Saline + SNT)

Data are represented as the mean ± SEM; **P* < 0.05, ****P* < 0.001, *****P* < 0.0001; Student's t test (b, d).

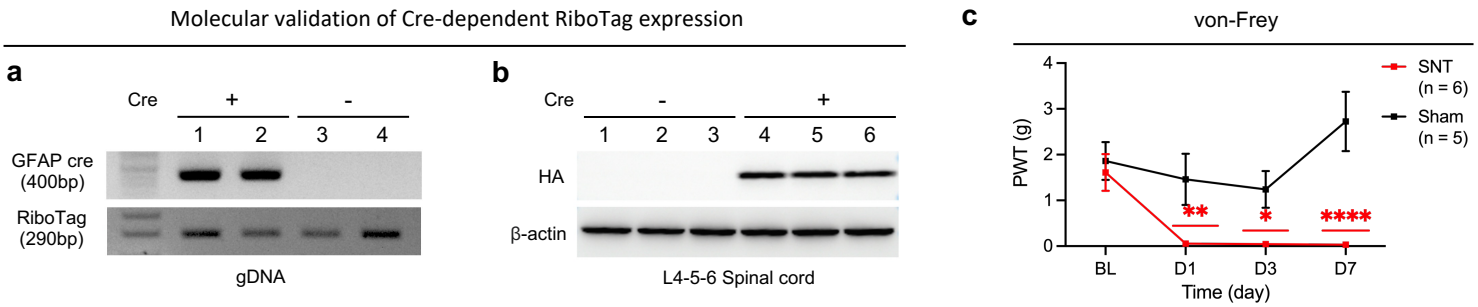


**Supplementary Figure 3. GFAP$^{cre+}$ x RPL22$^{HA/HA}$ RiboTag mice model validation.**

**a** PCR genotyping of tail-biopsy gDNA to detect the Cre transgene (400 bp) and the RiboTag (RPL22$^{HA}$) allele (290 bp). Lanes 1–2: Cre+; lanes 3–4: Cre-.

**b** Western blot of L4–L6 spinal cord lysates probed with anti-HA (top) to detect HA-tagged RPL22 and anti-β-actin (bottom) as loading control. Cre+ mice (lanes 1–2) show robust HA signal; Cre– mice (lanes 3–6) do not.

**c** von-Frey test of neuropathic pain model. Sham-operated (black, n = 5) and SNT (red, n = 6) mice, measured at baseline (BL) and days 1, 3, 7 post-surgery. **P = 0.0011 (D1 Saline + SNT verses Saline + Sham), *P = 0.0129 (D3 Saline + SNT verses Saline + Sham), ****P < 0.0001 (D7 Saline + SNT verses Saline + Sham)

Data are represented as the mean ± SEM; **P* < 0.05, ****P* < 0.001, *****P* < 0.0001; Two-way ANOVA-multiple comparisons test (c).

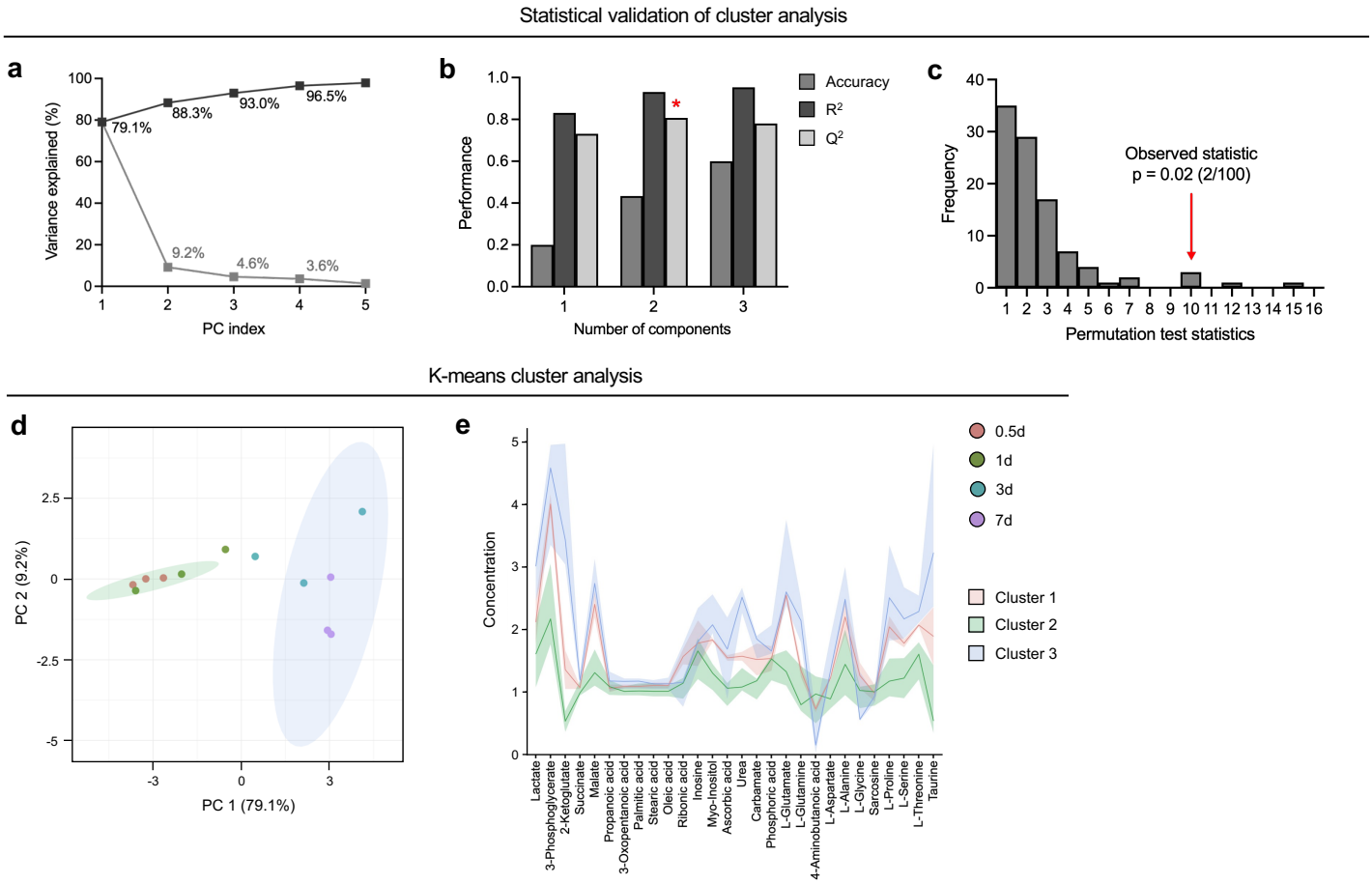


**Supplementary Figure 4. Statistical analysis of GC-MS metabolomics**

**a-c** Statistical validation of cluster analysis.

**a** Cumulative variance explained by successive principal components (PCs). PC 1 accounts for 79.1 % of the total variance, with PCs 2–5 contributing 9.2 %, 4.6 %, 3.6 % and < 1 %, respectively.

**b** Cross-validation performance of the PLS-DA model as a function of the number of latent components. Bars represent classification accuracy, goodness-of-fit ($R^2$), and predictive ability ($Q^2$). A red asterisk indicates the optimal model (two components) selected for downstream analysis.

**c** Permutation test (n = 100) of the PLS-DA classification statistic. The histogram shows the distribution of test statistics obtained under random class assignments; the red arrow denotes the observed statistic (p = 0.02, 2/100 permutations $\geq$ observed).

**d-e** K-mean cluster analysis of GC-MS metabolomics data.

**d** PCA score plot of individual samples colored by time point (0.5 d: red; 1 d: green; 3 d: teal; 7 d: purple), with 95 % confidence ellipses overlaid for the three K-means clusters identified. Axes are labeled with the percentage of variance explained by PC 1 (79.1 %) and PC 2 (9.2 %).

**e** Mean concentration profiles ($\pm$ SD shading) of metabolites within each of the three clusters, plotted across time points. Cluster 1 (salmon), Cluster 2 (light green) and Cluster 3 (light blue) show distinct temporal patterns, highlighting early-, intermediate- and late-responding metabolite groups.

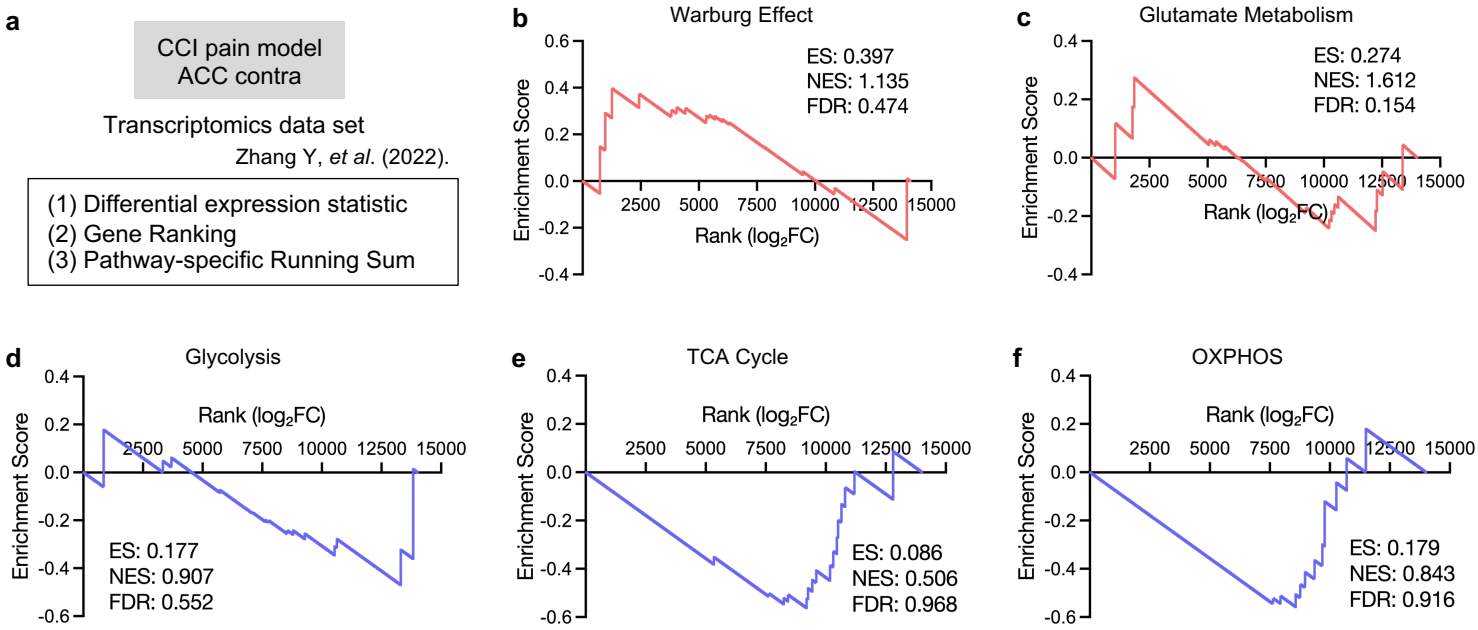


**Supplementary Figure 5. Cancer-associated metabolic pathways in energy metabolism identified by pathway gene profiling.**

**a** Experimental scheme of transcriptomics analysis in Chronic constriction injury (CCI) pain model. (Time point: 7day; fold change was normalized by Sham)

**b-f** Gene set enrichment analysis (GSEA) plot showing each pathway gene in CCI 7d (n = 3) verses Sham (n = 3).

**b** Warburg effect metabolism GSEA plot.

**c** Glutamate metabolism GESA plot.

**d** Glycolysis metabolism GSEA plot.

**e** TCA cycle GSEA plot.

**f** OXPHOS GSEA plot.

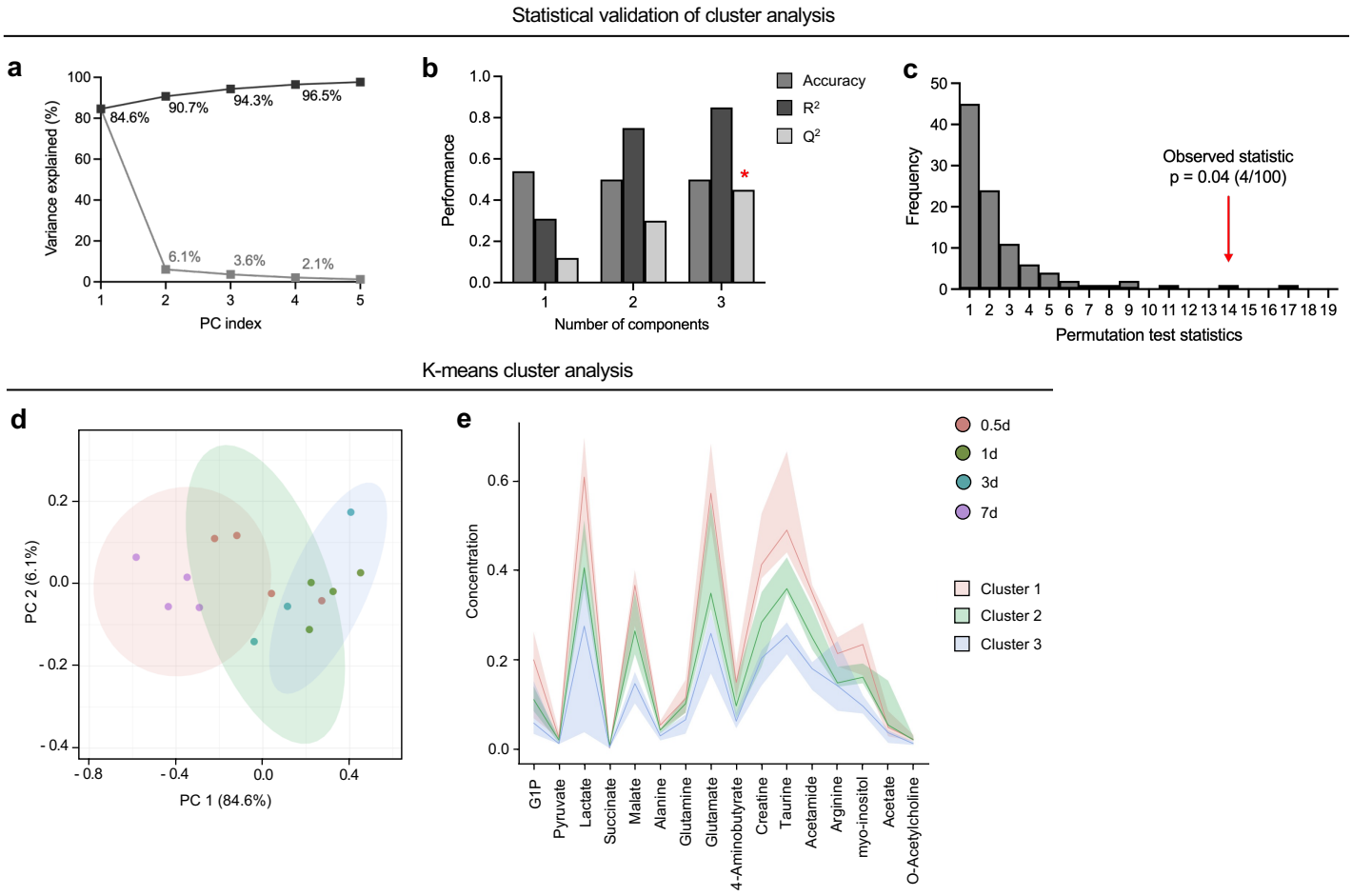


**Supplementary Figure 6. Statistical analysis of NMR metabolomics**

**a-c** Statistical validation of cluster analysis.

**a** Cumulative variance explained by successive PCs. PC 1 explains 84.6 % of the variance, with PCs 2–5 explaining 6.1 %, 3.6 %, 2.1 % and < 1 %, respectively.

**b** PLS-DA cross-validation metrics for one-, two- and three-component models. Light gray bars show accuracy, dark gray bars $R^2$, and white bars $Q^2$. The red asterisk marks the three-component model chosen for optimal balance of fit and prediction.

**c** Permutation testing (n = 100) of the PLS-DA statistic. The null distribution is shown as a histogram; the red arrow indicates the observed statistic (p = 0.04, 4/100 permutations $\geq$ observed).

**d-e** K-mean cluster analysis of NMR metabolomics data.

**d** PCA score plot of all samples, colored by time point (0.5 d: red; 1 d: green; 3 d: teal; 7 d: purple) with 95 % confidence ellipses for each of the three K-means clusters. PC 1 and PC 2 explain 84.6 % and 6.1 % of the variance, respectively.

**e** Cluster-specific mean concentration trajectories ($\pm$ SD shading) of representative metabolites (listed on the abscissa). Clusters are colored as in panel D: Cluster 1 (salmon), Cluster 2 (light green) and Cluster 3 (light blue), illustrating divergent temporal responses among metabolite groups.

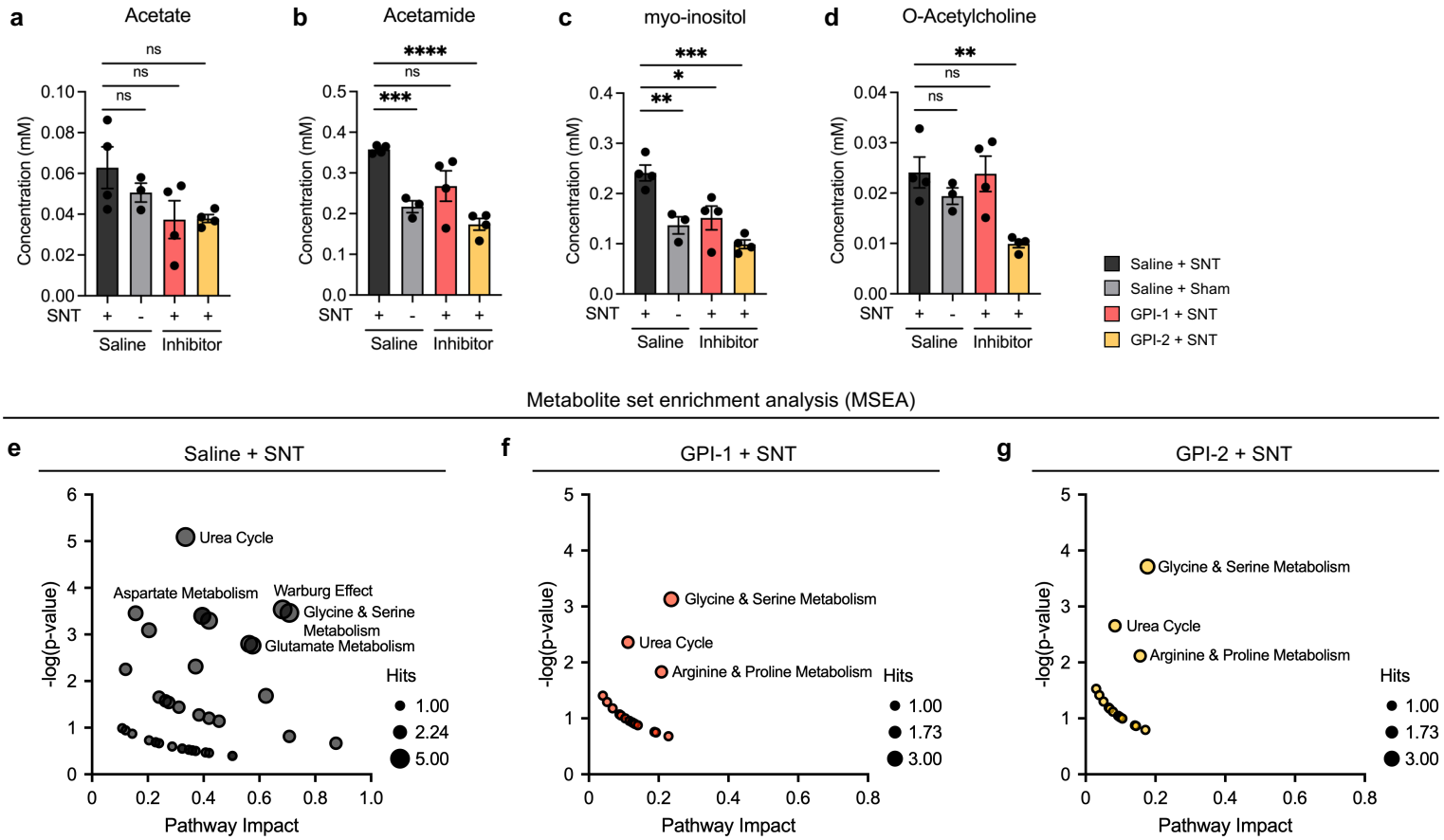


**Supplementary Figure 7. Inhibition of ACC glycogenolysis mediates decreased metabolic dynamics in chronic pain.**

**a-d** Metabolite concentration data by NMR analysis.

**a** Acetate concentration of each group.

**b** Acetamide concentration of each group. ***P = 0.0001 (Saline + Sham verse Saline + SNT), ****P < 0.0001 (GPI-2 + SNT verse Saline + SNT)

**c** Myo-inositol concentration of each group. **P = 0.0066 (Saline + Sham verse Saline + SNT), *P = 0.0197 (GPI-1 + SNT verse Saline + SNT), ***P = 0.0002 (GPI-2 + SNT verse Saline + SNT)

**d** O-Acetylcholine concentration of each group. **P = 0.0041 (GPI-2 + SNT verse Saline + SNT)

**e-g** Metabolite set enrichment analysis (MSEA) of NMR metabolomics data. Labeling selected high enrichment metabolic pathway.

**e** SNT after saline injection.

**f** SNT after GPI-1 injection.

**g** SNT after GPI-2 injection.

Data are represented as the mean ± SEM; *P < 0.05, **P < 0.01, ***P < 0.001, ****P < 0.0001; Student's t test (a-d). Pathway enrichment analysis of NMR data is performed using MetaboAnalyst v6.0. ([http://www.metaboanalyst.ca](http://www.metaboanalyst.ca/)).